Consequences of cAMP and Catalytic-Subunit Binding on the Flexibility of the A-Kinase Regulatory Subunit†

Fei Li,‡,§ Milind Gangal,‡,§ John M. Jones,|| Jason Deich,||,⊥ Kimberly E. Lovett,|| Susan S. Taylor,|| and David A. Johnson*,‡

Division of Biomedical Sciences, University of California, Riverside, California 92521-0121 and Howard Hughes Medical Institute, Department of Chemistry and Biochemistry, School of Medicine, University of California, San Diego, La Jolla, California 92093-0359

Received September 18, 2000; Revised Manuscript Received October 27, 2000

ABSTRACT: A combination of site-directed labeling and time-resolved fluorescence anisotropy was used to further elucidate the structure and underlying dynamic features of the type I regulatory (R^I_α) subunit of the cAMP-dependent protein kinase. Specifically, the consequences of cAMP and the catalytic (C)-subunit binding on the backbone flexibility around seven sites of cysteine substitution and fluorescein maleimide labeling (Thr^6Cys, $Leu^{66}Cys$, $Ser^{75}Cys$, $Ser^{81}Cys$, $Ser^{99}Cys$, $Ser^{145}Cys$, and $Ser^{373}Cys$) in the R^I_α subunit were assessed. Focusing on the fast rotational correlation time, the results indicate that most of the interdomain segment connecting the dimerization/docking (D/D) and tandem cAMP-binding domains is probably weakly associated with the latter domain. Also, this segment becomes more tightly bound to the C subunit upon holoenzyme formation. The results also suggest that there is a short 'hinge' segment (around $Leu^{66}Cys$) that could allow the structured interdomain/cAMP-binding and D/D domains to pivot about each other. Finally, cAMP binding dramatically reduces the backbone flexibility around only the two sites of cysteine substitution in the cAMP-binding domains, suggesting a selective structural stabilization caused by cAMP and a "tight" coupling of low-nanosecond fluctuations selectively within the tandem cAMP-binding domains.

Although it is a truism that conformational flexibility and dynamics play essential roles in protein activity, our knowledge of the flexibility and dynamics of most proteins is limited. For example, most of what is known about the flexibility and dynamics of the signaling protein cAMP-dependent protein kinase (cAPK)[1] centers around its monomeric catalytic (C) subunit. Substrate binding induces a narrowing of the C-subunit active-site cleft that is formed by its small and large lobes (*1*), type-II cAPK-regulatory (R^{II}) subunit binding mobilizes the N-terminus of the myristylated C subunit (*2*), and the heat-stable cAPK-inhibitor peptide, PKIα, undergoes a disorder−order transition upon binding to the C subunit (*3*).

With regard to the homodimeric R subunit, cAMP raises the concentration for chaotropic denaturation, indicating that cAMP stabilizes the R subunit. This also suggests that cAMP reduces all or part of its conformational flexibility (*4*). Small-angle scattering results suggest a hinge movement at each end of the R^{II} subunit dimerization/docking (D/D) domain, which links the two monomeric R subunits and forms the binding site for cAPK anchoring proteins (AKAPs) (*5*). The size and the inherent difficulty of crystallizing full-length isoforms of the R subunit have limited the utility of both NMR spectroscopy and X-ray crystallography for the analysis of its flexibility and dynamics. Some success has been achieved by studying fragments of the R subunit. The solution structure of the R^{II}_α-subunit D/D domain has been determined by multidimensional NMR spectroscopy (*6*). Similarly, a Δ1−91 deletion mutant C-terminal fragment of the cAMP-bound R^I_α subunit has been crystallized, and the structure of residues 113−376 has been determined (*7*). No portion of an R subunit that includes cAMP-binding domains has been crystallized either in the absence of cAMP or complexed to the C subunit. Consequently, the structural and dynamic consequences of either cAMP or C subunit binding on the R subunit has not been elucidated by X-ray crystallography.

To gain further insight into both the flexibility of the homodimeric R subunit and the structural consequences of

† This work was supported by a grant from the National Institutes of Health (GM 34921) to S.S.T.

* To whom correspondence should be addressed. E-mail: david.johnson@ucr.edu.

‡ Division of Biomedical Sciences.

§ These authors contributed equally to this work.

|| Howard Hughes Medical Institute.

⊥ Present address: Department of Chemistry, Stanford University, Stanford, CA 94305-5080.

[1] Abbreviations: cAPK, cAMP-dependent protein kinase; buffer A, 20 mM MOPS, 100 mM KCl, pH 7.1; buffer B, 20 mM MOPS, 100 mM KCl, 5 mM β-mercaptoethanol, pH 7.1; C subunit, the α isoform of the nonmyristylated catalytic subunit of cAPK; R subunit, regulatory subunit of cAPK; DTT, dithiothreitol; f_{xb}, fraction of the observed anisotropy decay associated with the "fast" depolarization processes; r_o, time zero anisotropy; $r_{very\ fast}$, difference between r_o of immobilized fluorescein (0.34) and the observed r_o; r_{fast}, amplitude of the "fast" anisotropy decay processes (equals $r_o \times f_{xb}$); r_{slow}, amplitude of the "slow" anisotropy decay processes (equals r_o minus r_{fast}); ϕ_{fast}, fast rotational correlation time; ϕ_{slow}, slow rotational correlation time; SDL, site-directed labeling; TRFA, time-resolved fluorescence anisotropy.

10.1021/bi002196l CCC: $19.00
Published on Web 11/21/2000

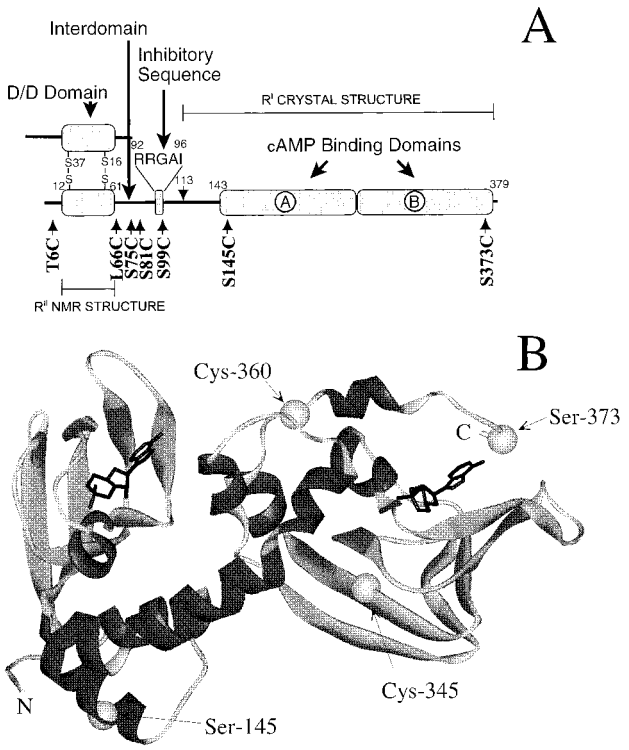

FIGURE 1: Structure of the R subunit with the sites of mutation. (A) The positions of the seven X-to-Cys mutants are indicated with an arrow. (B) Positions of sites of mutation (S145C and S373C), native cysteines, and cAMP molecules are highlighted on the crystal structure of Δ^{1-91} R^{I}_{α} deletion mutant.

cAMP and C-subunit binding, we used a combination of site-directed labeling (SDL) and time-resolved fluorescence anisotropy (TRFA) to map the backbone flexibility of the R^{I}_{α} subunit alone and complexed to either the C subunit or cAMP. Specifically, seven full-length single-site X-to-Cys R^{I}_{α} mutants were prepared. The seven sites of cysteine substitution, illustrated in Figure 1, include (i) a site ($Thr^{6}Cys$) between the N-terminus and the D/D domains (residues 12−61), (ii) three sites ($Leu^{66}Cys$, $Ser^{75}Cys$, and $Ser^{81}Cys$) in the interdomain region between the D/D domain and inhibitory sequence (residues 94−98), (iii) a site ($Ser^{99}Cys$) between the inhibitory sequence and the tandem cAMP-binding domains, and (*iv*) two sites in the cAMP-binding domains, one ($Ser^{145}Cys$) within the C-subunit recognition domain on the B helix of the low-affinity cAMP binding domain ("A" domain) and the other ($Ser^{373}Cys$) on the C-terminal segment that caps the high-affinity cAMP binding site in the "B" domain. The substituted cysteines were selectively conjugated to fluorescein maleimide (FM), and the time course of the emission anisotropy of these conjugates was measured in the absence and presence of the C subunit and cAMP. The results are consistent with the homodimeric R^{I}_{α} subunit, both alone and complexed to the C subunit, existing as two large globular domains connected to the structured D/D domains by a short, flexible hinge region around Leu^{66}. Also, the results suggest that the structural stabilizing effects of the cAMP are confined to the tandem cAMP-binding domains.

EXPERIMENTAL PROCEDURES

Preparation and Purification of the Mutant C Subunits. Seven R^{I}_{α}-subunit mutants (T6C, L66C, S75C, S81C, S99C, S145C, and S373C) were prepared as described previously (*8*). The S145C mutant contained two additional point mutations, C16A and C37S, in the D/D domain that eliminated the dimerization disulfide bonds but do not block dimer formation at or below physiological ionic strength (*8*). The recombinant nonmyristylated wild-type C was prepared as described elsewhere (*9*).

Fluorescein Maleimide Labeling. With the exception of the S75C and S81C mutants, the R-subunit samples (12.5−25 nmol) were initially buffer exchanged by elution through a G-25 column (1.5 × 7 cm) equilibrated with buffer A (20 mM MOPS, 100 mM KCl, pH 7.1). The protein fractions were pooled and the concentration of the pooled samples were determined with UV−vis spectrometry using an ϵ_{280} of 48 000 M^{-1} cm^{-1}. To minimize labeling of the native cysteines, cAMP (100 μM) was added to the reaction mixture before the addition of a near stoichiometric amount (0.8 mol of FM/ mol of protein) of FM. The protein concentration of the reaction mixture ranged between 3 and 6 μM. The reactions were allowed to proceed for 1 h at room temperature, protected from light, and then eluted through a Sephadex G-25 column (2.5 × 6 cm) followed by a Sephacryl S-200 column (2.5 × 7 cm) equilibrated with buffer B (20 mM MOPS, 100 mM KCl, 5 mM β-mercaptoethanol, pH 7.1) at room temperature. Fluorescein emission (excitation at 470 nm and emission at 525 nm) from the column fractions was measured, and the fluorescent fractions with retention times that corresponded to unmodified R subunit were pooled. Aliquots of the pooled fractions were subjected to gel electrophoresis under denaturing conditions (12% SDS−PAGE) (*10*) and the fluorescent bands were visualized with a mineral lamp to assess whether any unconjugated fluorescein was associated with the R mutants. Because of the limited reactivity of FM toward the free S75C and S81C mutants, it was necessary to complex these mutants to the C subunit prior to the labeling. This was accomplished by first combining a 1.2-fold molar excess of C subunit with 1 mg of the R subunit and then dialyzing the mixture overnight prior to starting the labeling protocol described above. The R subunit was separated from the C subunit by the addition of cAMP (100 μM) to the elution buffer of a Sephacryl S-200 column (1.5 × 25 cm).

Phosphotransferase Assay. The activity of the labeled R mutants was evaluated by assessing its ability to inhibit the phosphotransferase activity of recombinant C subunit using the method of Cook et al. (*11*) with kemptide as a substrate.

Determination of the Stoichiometry of Labeling. The stoichiometry of FM-labeled R subunits (F_{total}) was determined spectrophotometrically by substitution of the measured absorbance values at 280 nm (A_{280}) and 497 nm (A_{497}) into the expression

$$\frac{[\text{Fluorescein}]}{[\text{R Subunit}]} = \frac{A_{497}/83\,000}{(A_{280} - 0.18A_{497})/48\,000} \qquad (1)$$

The fraction of the protein that was specifically labeled ($F_{specific}$)was estimated with the expression

$$F_{specific} = F_{total} - F_{nonspecific} \qquad (2)$$

where $F_{nonspecific}$ is fraction of the protein that is labeled in the absence of any specific labeling, i.e., when wt-protein is

labeled. This assumes that the nonspecific labeling reaction is much faster than the specific reaction.

Removal of cAMP from R Subunits. One milliliter of cAMP-agarose 6% (Sigma Corp, St. Louis; catalog no. A-7775) that had been equilibrated with buffer B was combined with 2 mL of labeled protein (2−4 μM) and incubated at 4 °C overnight. In the morning, the excess buffer was aspirated off, and the resin was then washed twice with buffer B at room temperature. The FM-labeled R subunit was released from the resin by incubation of the protein/resin complex for 0.5 h at room temperature with buffer C (20 mM MES, 100 mM KCl, pH 5.1) that included cGMP (25 mM). The released protein was then dialyzed overnight at 4 °C against three 1 L changes of buffer B or was used directly to form holoenzyme.

Formation of Holoenzyme. The labeled R mutants (0.5 μM) were combined with a 10-fold excess of recombinant C subunit and then dialyzed overnight at 4 °C against 1 L (times 3) of buffer B that contained 1 mM $MgCl_2$ and 0.2 mM ATP.

Steady-State Emission Spectra. Steady-state emission spectra were measured at room temperature using a Instrument S. A., Inc. Jobin Yvon/Spex FluoroMax II spectrofluorometer with the excitation and emission band widths set at 5 nm.

Time-Resolved Fluorescence Anisotropy. The time-resolved emission anisotropy was determined by time-correlated single photon-counting (*12*) with an IBH (Edinburgh, U.K.) NanoLED flash lamp run at 1 MHz and IBH model TBX-04 photon detector. The vertically [$I_{||}(t)$] and orthogonally [$I_{\perp}(t)$] polarized emission components were collected by exciting samples with vertically polarized light while orienting the emission polarizer (Polaroid HNP′B dichroic film) in either a vertical or orthogonal direction. Excitation and emission bands were selected with an Oriel 500-nm short-pass interference (catalog no. 59876) and a Corning 3-68 cuton or Omega Optical 530-DF-35 interference filter, respectively. Typically, 2×10^4 peak counts were collected (in 1−2 min) when the emission polarizer was vertically oriented. The orthogonal emission decay profile was generated in the same amount of time as that used to generate the vertical emission decay profile. The samples were held at 22 °C. To minimize convolution artifacts, flash lamp profiles were recorded by removing the emission filter and monitoring light scatter from a suspension of latex beads. The wavelength-dependent temporal dispersion of the photoelectrons by the photomultiplier was corrected by the data analysis software. The polarization bias (G) of the detection instrumentation was determined by measuring the integrated photon counts/6×10^6 lamp flashes that were detected while the samples were excited with orthogonally polarized light and the emission monitored with a polarizer oriented in the vertical and orthogonal directions ($G = 1.028$).

The emission anisotropy, $r(t)$, is given by the expression

$$r(t) = \frac{I_{||}(t) - G \cdot I_{\perp}(t)}{I_{||}(t) + 2G \cdot I_{\perp}(t)} \quad (3)$$

From this and the expression for the total emission for a macroscopically isotropic sample,

$$S(t) = I_{||}(t) + 2G \cdot I_{\perp}(t) \quad (4)$$

the individual polarized components can be expressed as

$$I_{||}(t) = \frac{S(t)}{3}[1 + 2r(t)] \quad (5)$$

and

$$I_{\perp}(t) = \frac{S(t)}{3}[1 - r(t)] \quad (6)$$

Thus, both $I_{||}(t)$ and $I_{\perp}(t)$ are determined by the same fitting functions, $S(t)$ and $r(t)$, and fitting parameters.

The fluorescence lifetimes for each sample were determined by initially generating a total emission profile from $I_{||}(t)$ and $I_{\perp}(t)$ with eq 4, and then fitting this decay profile to a biexponential decay expression with the Globals Unlimited (Laboratory for Fluorescence Dynamics, Urbana, IL) software package (*13*). The resulting lifetimes were entered and fixed in the second step of the analysis process where $I_{||}(t)$ and $I_{\perp}(t)$ were simultaneously analyzed for the parameters of $S(t)$ and $r(t)$ (with the Globals Unlimited program). Here, $r(t)$ is a nonassociative anisotropy decay function

$$r(t) = r_o f_{xb} \exp(-t/\varphi_{fast}) + r_o(1 - f_{xb}) \exp(-t/\varphi_{slow}) \quad (7)$$

where r_o is the amplitude of the anisotropy at time zero, f_{xb} is the fraction of the anisotropy decay associated with the fast decay processes, and ϕ is the rotational correlation time of the anisotropy decay. The subscripts *fast* and *slow* denote the fast and slow decay processes, respectively. This nonassociative model indicates that the rotational correlation times are common to each of the emission relaxation times. Goodness of fit was evaluated from the value of χ^2 and visual inspection of the difference between the experimental data and the empirical anisotropy decay model.

Because of the large difference between the reporter group emission lifetime (~4 ns) and the estimated whole-body rotational correlation times (82−110 ns) of the R^I-subunit configurations examined, ϕ_{slow} is ill defined. Consequently, a range (not a mean ± SD) of ϕ_{slow} values was determined for each data set that produced a reasonably acceptable fit to the anisotropy decay. Specifically, a unidimensional search procedure was performed that involved directed searches along the ϕ_{slow} parameter axis, not allowing other fitting parameters to vary, to find the minimum and maximum ϕ_{slow} values that raised the χ^2 values by 5%.

RESULTS

Labeling and Characterization of R^Ia Subunit Mutants. The seven mutant proteins were labeled and purified as described under Experimental Procedures. Parallel FM labeling reactions, carried out with recombinant wt-R^I instead of mutant proteins, showed detectable nonspecific labeling when quantified spectrophotometrically. Alone or complexed with the C subunit, the wt-R^I subunit was associated with about the same level of nonspecific labeling (2.6−2.9%). The total labeling stoichiometry (probe:R^I subunit) for FM-T6C, FM-L66C, FM-S75C, FM-S81C, FM-S99C, FM-S145C, and FM-S373C was 0.27, 0.54, 0.11, 0.37, 0.37, 0.47, and 0.52, respectively. Assuming that the nonspecific labeling reaction is faster than the specific labeling reaction, the percent of the specific labeling for FM-T6C, FM-L66C, FM-

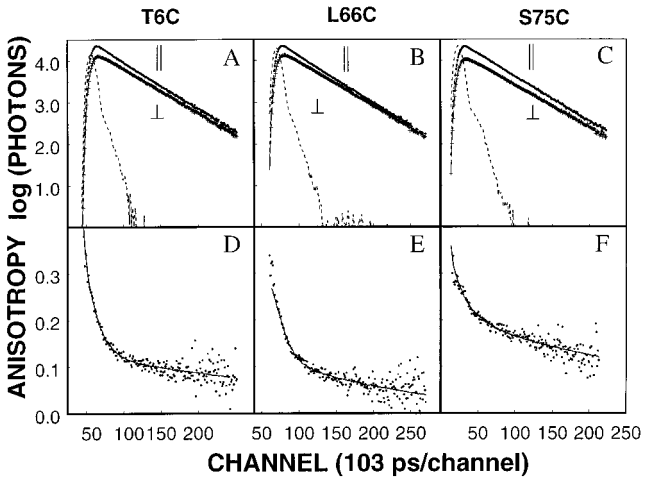

FIGURE 2: Emission and anisotropy decay of cAMP-bound FM-T6C, FM-L66C, FM-S75C. Panels A−C illustrate the parallel (||) and perpendicular (⊥) emission decays (single datum points), a smooth line through these points was generated with the best-fit parameters for a biexponential decay function, and the flash lamp profile (dashed lines) for cAMP-bound FM-T6C (A), FM-L66C (B), and FM-S75C (C). Panels D−F show the time-resolved anisotropy decay (single datum points) and a smooth line through these points generated with the best-fit parameters (Table 1) for a double exponential nonassociative anisotropy decay model (eq 7) for FM-T6C (D), FM-L66C (E), and FM-S75C (F). The fits are shown with the start of the fit being the channel with 10% of the maximal counts. The concentration of all labeled R proteins was between 200 and 300 nM.

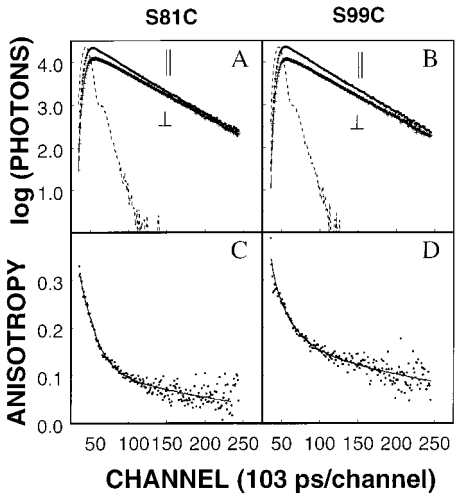

FIGURE 3: Emission and anisotropy decay of cAMP−bound FM-S81C and FM-S99C. Panels A and B illustrate the parallel (||) and perpendicular (⊥) emission decays (single datum points), a smooth line through these points was generated with the best-fit parameters for a biexponential decay function, and the flash lamp profile (dashed lines) FM-S81C (A) and FM-S99C (B). Panels C and D show the time-resolved anisotropy decay (single datum points) and a smooth line through these points generated with the best-fit parameters (Table 1) for a double exponential nonassociative anisotropy decay model (eq 7): FM-S81C (C) and FM-S99C (D). See the legend of Figure 2 for more details.

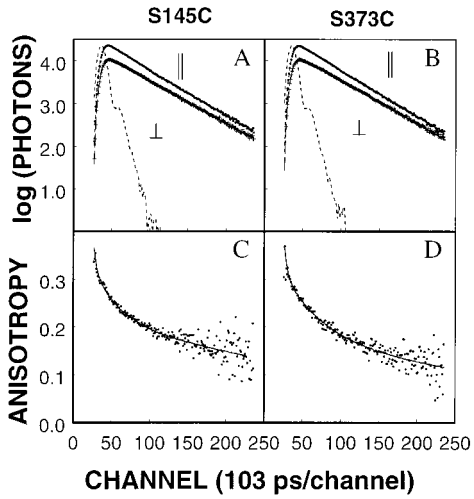

FIGURE 4: Emission and anisotropy decay of cAMP−bound FM-S145C* and FM-S373C. Panels A and B illustrate the parallel (||) and perpendicular (⊥) emission decays (single datum points), a smooth line through these points was generated with the best-fit parameters for a biexponential decay function, and the flash lamp profile (dashed lines) for FM-S145C (A) and FM-S373C (B). Panels C & D show the time-resolved anisotropy decay (single datum points) and a smooth line through these points generated with the best-fit parameters (Table 1) for a double exponential nonassociative anisotropy decay model (eq 7) for FM-S145C (C) and FM-S373C (D). See the legend of Figure 2 for more details. (*FM-S145C is a triple mutant S145C/C16A/C37S.)

S75C, FM-S81C, FM-S99C, FM-S145C, and FM-S373C was 89, 95, 76, 93, 92, 97, and 94%, respectively.

The emission maxima of the labeled mutants following the Sephacryl S-200 chromatography step were about the same and ranged between 517 and 520 nm. With the exception of the S99C mutant, which does not bind to the C subunit (*14*), all labeled mutants inhibited recombinant C subunit phosphotransferase activity following the removal of the cAMP from the R^I_α mutants. This inhibition was reversed by the addition of cAMP, indicating the labeling did not significantly affect the functional activity of the labeled mutants (data not shown).

Emission and Anisotropy Decay. The time-resolved emission and anisotropy decay profiles of FM-T6C, FM-L66C, FM-S75C, FM-S81C, FM-S99C, FM-S145C, and FM-S373C before removal of cAMP are illustrated in Figures 2−4, and the best-fit anisotropy decay parameters and the geometric average lifetimes are summarized in Table 1. The emission decay kinetics of each labeled mutant were well fit to a biexponential decay model. For simplicity only the geometric averaged lifetimes are shown in Table 1 and ranged between 3.94 and 4.21 ns. The actual range of the short and long emission lifetimes for the various cAMP-bound mutants were 4.18−4.45 ns and 1.31−2.83 ns, respectively, with the amplitudes of the longer component contributing between 77 and 89% of the total decay amplitude (data not shown).

The $I_{||}(t)$ and $I_{\perp}(t)$ emission profiles were fit to a model-free nonassociative biexponential equation (eq 6). With the exception of the FM-S373C mutant, the whole-body rotational correlation time predicted by the Stokes−Einstein equation (82 ns) using the previously published hydrodynamic radius of the cAMP-bound R^I_α subunit (43 Å) (*15*) is greater than the observed values (24−62 ns) of the slower of the two observed rotational correlation times (ϕ_{slow}). This difference may (1) represent the inherent difficulty of using FM to accurately monitor rotational correlation times that are greater than 10 times its emission lifetime, (2) suggest the existence of intermediate rate fluctuation processes, between the fast and slow rotational diffusion, and/or (3) reflect the tendency for the faster of a cluster of slow rotational correlation times to dominate the observed cor-

Table 1: Effect of cAMP and C Subunit on the Anisotropy Decay Parameters of FM-Labeled R Mutants[a]

mutant and condition	r_o[b]	f_{xb}[c]	$r_{very\ fast}$[d]	r_{fast}[e]	ϕ_{fast}[f] (ns)	ϕ_{slow}[g] (ns)	χ^2	$\langle\tau\rangle$[h] (ns)
R^I_α alone								
FM-T6C	0.27 ± 0.01	0.45 ± 0.01	0.07 ± 0.01	0.12 ± 0.01	1.3 ± 0.3	38−59	1.2 ±0.2	3.91 ± 0.04
FM-L66C	0.25 ± 0.01	0.54 ± 0.06	0.09 ± 0.02	0.14 ± 0.01	1.2 ± 0.1	19−34	2.2 ± 1.1	3.67 ± 0.14
FM-S75C	nd	nd	nd	nd	nd	nd	nd	nd
FM-S81C	0.27 ± 0.01	0.49 ± 0.02	0.07 ± 0.01	0.13 ± 0.01	1.7 ± 0.1	26−40	1.5 ± 0.1	4.12 ± 0.01
FM-S99C	0.28 ± 0.01	0.32 ± 0.01	0.06 ± 0.01	0.09 ± 0.01	1.9 ± 0.5	31−41	1.1 ± 0.1	3.71 ± 0.02
FM-S145C[i]	0.29 ± 0.01	0.21 ± 0.01	0.05 ±0.01	0.06 ± 0.01	2.1 ± 0.2	33−47	1.4 ± 0.1	3.90 ± 0.01
FM-S373C	0.27 ± 0.01	0.22 ± 0.02	0.07 ±0.01	0.06 ± 0.01	2.5 ± 0.4	47−68	1.6 ± 0.1	4.18 ± 0.01
R^I_α:cAMP$_4$								
FM-T6C	0.26 ± 0.01	0.46 ± 0.01	0.08 ± 0.01	0.12 ± 0.01	1.5 ± 0.2	39−62	1.1 ± 0.1	3.94 ± 0.02
FM-L66C	0.25 ± 0.02	0.44 ± 0.04	0.09 ± 0.02	0.11 ± 0.01	1.2 ± 0.1	24−37	1.2 ± 0.1	3.97 ± 0.02
FM-S75C	0.29 ± 0.01	0.28 ± 0.02	0.05 ± 0.01	0.08 ± 0.01	2.8 ± 0.4	36−49	1.2 ± 0.1	4.10 ± 0.03
FM-S81C	0.28 ± 0.01	0.50 ± 0.02	0.06 ± 0.01	0.14 ± 0.01	1.7 ± 0.1	27−38	1.3 ± 0.1	4.30 ± 0.01
FM-S99C	0.28 ± 0.01	0.36 ± 0.02	0.06 ± 0.01	0.10 ± 0.01	2.3 ± 0.3	33−44	1.2 ± 0.1	4.12 ± 0.01
FM-S145C[i]	0.30 ± 0.01	0.22 ± 0.02	0.04 ± 0.01	0.07 ± 0.01	3.2 ± 0.1	39−52	1.4 ± 0.1	4.02 ± 0.01
FM-S373C	0.31 ± 0.01	0.27 ± 0.02	0.03 ± 0.01	0.08 ± 0.01	4.6 ± 0.8	60−89	1.5 ± 0.1	4.21 ± 0.01
R^I_α:C$_2$								
FM-T6C	0.28 ± 0.01	0.42 ± 0.01	0.06 ± 0.01	0.12 ± 0.01	0.9 ± 0.1	62−96	1.2 ± 0.2	3.88 ± 0.02
FM-L66C	0.25 ± 0.01	0.47 ± 0.04	0.09 ±0.01	0.12 ± 0.01	1.3 ± 0.4	24−43	1.7 ± 0.4	3.73 ± 0.03
FM-S75C	0.31 ± 0.01	0.24 ± 0.01	0.03 ± 0.01	0.07 ± 0.01	3.9 ± 0.3	53−82	1.2 ± 0.1	4.14 ± 0.01
FM-S81C	0.30 ± 0.01	0.21 ± 0.03	0.04 ± 0.01	0.06 ± 0.01	4.4 ± 1.1	70−121	1.4 ± 0.1	4.23 ± 0.01
FM-S99C	nd	nd	nd	nd	nd	nd	nd	nd
FM-S145C[i]	0.33 ± 0.02		0.01 ± 0.02			82−142	1.3 ± 0.1	2.68 ± 0.01
FM-S373C	0.28 ± 0.01	0.17 ± 0.03	0.06 ± 0.01	0.05 ± 0.01	3.2 ± 0.7	54−80	1.5 ± 0.1	4.07 ± 0.02

[a] The results represent the mean (± SD) of at least three determinations. The vertically and orthogonally polarized emission decays were simultaneously analyzed for the parameters of $S(t)$ (eq 4) and $r(t)$ (eq 7) with the Globals Unlimited computer program. The experimental details are described under Experimental Procedures. Labeled-R subunit was present at a concentration between 200 and 300 nM. ATP (0.2 mM) and $MgCl_2$ (1 mM) were present in all samples containing C subunit. The temperature of all samples was held at 22 °C. [b] The time zero anisotropy. [c] The fraction of the observed anisotropy decay associated with the "fast" depolarization processes. [d] The amplitude of the "very fast" decay process which equals the anisotropy of immobilized fluorescein (0.34) minus r_o. [e] The amplitude of the "fast" anisotropy decay processes (equals $r_o \times f_{xb}$). [f] Fast rotational correlation time. [g] The range of the "slow" rotational correlation times that yielded χ^2 values 5% above the minimum. [h] Geometric average of two lifetimes. [i] FM-S145C is a triple mutant S145C/C16A/C37S.

relation time when the probe's lifetime is very much shorter than the rotational correlation times. The values of the fast rotational correlation times (ϕ_{fast}), which normally are reflective of the local backbone flexibility around each site of cysteine substitution and FM labeling (*16*), ranged from 1.2 to 4.6 ns (Table 1). With the exception of FM-T6C and FM-L66C, the magnitude of the ϕ_{fast} values (1.7−4.6 ns) are comparable to what was previously observed for ordered surface sites that are associated with sufficient electron density for structural determinations to be made from the crystalline C subunit (*16*). Also, the position of Leu^{66}, adjacent to the D/D domain, and the low ϕ_{fast} value of the FM-L66C mutant suggests that the area around Leu^{66} is very flexible and, therefore, may be part of a "hinge"; however, the existence of a flexible ω loop cannot be ruled out.

Effect of Removal of cAMP. The effects of cAMP removal on the time-resolved anisotropy decay were mutant dependent. Of the six FM-labeled mutants that could be examined, cAMP removal only significantly affected the anisotropy decay of FM-S145C and FM-S373C. The emission and anisotropy decay of the FM-T6C mutant were totally unaffected by cAMP removal. For FM-L66C, FM-S81C, and FM-S99C, cAMP removal reduced the averaged fluorescence lifetimes and from 3.97 to 3.60 ns, 4.30 to 4.12 ns, and 4.12 to 3.71 ns, respectively (Table 1), indicating that cAMP induced a change in the microenvironment around the reporter group without producing a detectable change in the backbone flexibility, in the interdomain between the D/D and cAMP binding domains. For FM-S145C and FM-S373C, cAMP removal decreased the ϕ_{fast} from 4.6 to 2.5 ns and 3.2 to 2.1 ns, respectively (Table 1), indicating that cAMP reduces the backbone flexibility around these two sites of cysteine substitution and FM labeling in the cAMP-binding domains. The cAMP-induced reduction in backbone flexibility occurred without affecting the segmental flexibility around the other mutated sites in the interdomain region and around Thr^{6}Cys at the N-terminus, suggesting there is little or no linkage of the low-nanosecond fluctuations between the N-terminus to around Ser^{81} and the cAMP-binding domains. (The anisotropy decay of cAMP-free FM-S75C was not determined, due to the low level of FM labeling and protein recovery following removal of cAMP.)

With the exception of the FM-S373C mutant, removal of cAMP had no significant effect on the ϕ_{slow} values. For the FM-S373C mutant, cAMP removal reduced the range of the ϕ_{slow} values from 60 to 89 ns to 47−68 ns, suggesting of the existence intermediate rate fluctuations between the slow and fast depolarization precesses. This, of course, needs to be confirmed with a longer-lifetime reporter group.

Effect of C-Subunit Binding. The effects of holoenzyme formation were associated with an increase in the ϕ_{slow} values. Relative to the cAMP-free configuration, the range of the ϕ_{slow} values increased from 19 to 68 ns to 24−142 ns. The smallest increase in the range of ϕ_{slow} values was associated with the FM-L66C mutant, the range only shifted from 19 to 34 ns to 24−43 ns. Given the very limited capacity of a 4-ns reporter group to monitor the rotational diffusion of a large macromolecular complexes, the observed ϕ_{slow}s of the holoenzymes are in reasonable agreement with that predicted by the Stokes−Einstein equation (110 ns) using the published hydrodynamic radius of the type I holoenzyme [47.4 Å (*17*)]. The low range of ϕ_{slow} values of the FM-L66C mutant in all

measured configurations suggests significant intermediate rate depolarization processes, but, again, this needs to be confirmed with a longer-lifetime reporter group.

Although C-subunit binding had no effect on the emission maxima of the labeled mutants that could be examined, it was associated with complex, mutant-dependent effects on the ϕ_{fast} values and emission lifetimes. For FM-T6C and FM-L66C, holoenzyme formation had no significant effect on either ϕ_{fast} or emission lifetime (Table 1), indicating that C-subunit binding to R^I_α does not affect the backbone flexibility around the N- and C-terminal residues that flank the D/D domain. However, for FM-S75C and FM-S81C, C-subunit binding was associated with a significant increase in the ϕ_{fast} values (2.8−3.9 ns and 1.7−4.4 ns, respectively; Table 1), indicating that C-subunit decreased the backbone flexibility around these sites (Table 1). For FM-S145C, holoenzyme formation was associated with a large decrease in the geometric average lifetime from 4.02 to 2.68 ns, and an immobilization of the reportor group such that it was no longer possible to resolve the anisotropy decay into two components (Table 1). These results indicate that holoenzyme formation was associated with a large reduction of the rotational freedom and change in the microenvironment of the FM attached to Ser[145]Cys, suggesting a sandwiching of the reporter group between the R^I_α and C subunits or an insertion of the conjugated FM into a crevice in the R^I_α subunit. This is consistent with mutational analysis that shows residues near Ser[145] (*18*) directly interact with the C subunit. For FM-S373C, holoenzyme formation was associated with a nonsignificant increase (relative to R^I_α alone) in the ϕ_{fast} value (2.5 ± 0.4 to 3.2 ± 0.7 ns) and a small decrease in the averaged emission lifetime (4.18 ± 0.01 to 4.07 ± 0.02 ns), suggesting a C-subunit induced conformational change around Ser[373]Cys but not a detectable change in backbone flexibility.

DISCUSSION

A combination of SDL and TRFA was used to measure the structural consequences of cAMP and C-subunit binding on the conformational flexibility of the R^I_α subunit of cAPK. The measure of backbone flexibility here is the "fast" rotational correlation time (ϕ_{fast}) at each site of cysteine substitution and fluorescein labeling. ϕ_{fast} is inversely correlated to the average main-chain atom temperature factors around each site of fluorescein labeling (about ±4 residues) (*16*). (The r_{fast} values were previously observed to be less well correlated to the temperature factors; consequently, little attention is given them here.) Although there are only a limited number of examples, the meaning of ϕ_{fast} values comes from a comparison of crystallographic and SDL/TRFA results. In the analysis of the nonmyristylated C subunit of cAPK (*16*), the ϕ_{fast} values at two sites (FM-Lys[16]Cys and FM-Cys[343]) near the N- and C-termini, which are weakly anchored to the core catalytic domain, are 1.9 and 2.0 ns, respectively. Importantly, these two sites are associated with high-temperature factors and are near nonresolved residues in the crystallographic structure (*19*). N-Terminal myristylation of the C subunit, which stabilizes the N-terminus to the core catalytic domain (*20*), shifts the ϕ_{fast} value of the FM-labeled Lys[16]Cys from 1.9 to 2.9 ns (*2*). Furthermore, the ϕ_{fast} values of two additional sites of Cys-substitution (Ala[6]Cys and Gly[9]Cys) that are in a region where there is insufficient electron density for crystallographic structural determination, are 1.4 and 1.5 ns, respectively (unpublished results). Surface sites that interact more with the core domains are associated with ϕ_{fast} values greater than about 1.8 ns. For example, a site in the large lobe of the C subunit (Ile[244]Cys) is associated with a ϕ_{fast} value of 2.8 ns in both the so-called "open" and "closed" conformations of the C subunit. Similarly, Lys[81]Cys at the tip of the small lobe is associated with a ϕ_{fast} value of 2.3 ns in the "open" and 3.2 ns in the "closed" conformation of the C subunit. In this report, the two sites of SDL (Ser[145]Cys and Ser[373]Cys) are in a region in which crystallographic structural information exists (*7*), and the ϕ_{fast} values are 3.2 and 4.6 ns, respectively (Table 1). These observations suggest that ϕ_{fast} values below about 1.7 ns are associated with unstructured areas that do not have sufficient electron density to allow crystallographic structural determination, and ϕ_{fast} values from about 1.9 ns and above are associated with increasingly ordered structural elements.

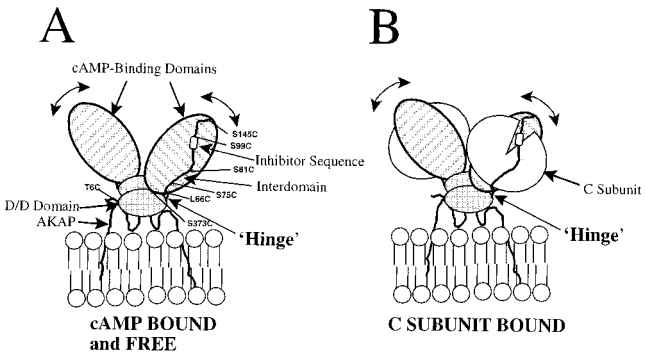

FIGURE 5: Schematic structure of the R subunit free (A), cAMP-bound (A), and complexed to the C subunit (B).

Using the above interpretation of the ϕ_{fast} values, the structural character of the N-terminal region of the cAMP-bound R^I_α subunit can be deduced. First, around the two sites of SDL that flank the structured D/D domain, the ϕ_{fast} values of Thr[6]Cys and Leu[66]Cys are both <1.5 ns, which indicates that these segments are relatively flexible and do not interact strongly with other structural elements. In contrast, around Ser[75]Cys, Ser[81]Cys, and Ser[99]Cys, the ϕ_{fast} values are higher (2.8, 1.7, and 2.3 ns, respectively) indicating less segmental flexibility particularly around Ser[75]Cys and Ser[99]Cys and thus a weak interaction with a structured domain, i.e., the cAMP-binding domains and/or the D/D domain. The two sites of SDL in cAMP-binding domains (Ser[145]Cys and Ser[373]Cys) are associated with relatively high ϕ_{fast} values as expected from the crystallographic structure of the Δ1−91-R^I deletion mutant (*7*). Taken together, the results indicate that the interdomain from, at least, Ser[75] to Ser[99] is weakly associated with another part of the molecule. Furthermore, the results point to the existence of a short, flexible segment around Leu[66] at the C-terminal side of the structured D/D domain that could allow the interdomain/cAMP-binding region to pivot about the D/D domain.

This arrangement of R^I-subunit domains, anchored to the lipid membrane via an AKAP, is illustrated in Figure 5. The inhibitory sequence (and much of the interdomain) is weakly associated with the tandem cAMP-binding domains and, consequently, is capable of slipping into the active-site cleft of the C subunit to inhibit its phosphotransferase activity. A

short hinge segment is also shown linking the structured D/D domain and the interdomain/inhibitory sequence/cAMP-binding region. This hinge region is equally flexible whether cAMP, C subunit, or RPP7, a 125-mer AKAP fragment of D-AKAP1 [21], are bound, because these agents have no effect on the ϕ_{fast} of the FM-L66C mutant (RPP7 data not shown). The mobility afforded by this arrangement could facilitate phosphorylation of adjacent membrane-associated targets. It should be noted that a mutant with two alanines substituted into the interdomain, R^I_α(R94A/R95A), shows less affinity for D-AKAP1 relative to wt-R^I_α, which suggests that a portion of the interdomain interacts directly with D-AKAP1 or contributes to the domain organization of R^I_α (*8*).

The probable association of the interdomain from, at least, Ser^{75} to Ser^{99} with the cAMP-binding domains is consistent with the observation that deletion of the first 91 residues of the R^I_α subunit produces a 100-fold increase in the rate of inhibition of the C-subunit catalytic activity by cAMP-bound R^I_α subunit (*17*). This 100-fold enhancement of the rate of inhibition would occur if the inhibitory sequence is anchored to the cAMP-binding domains by a segment of the interdomain creating steric hindrance for C-subunit access. Deletion of the N-terminal 91 residues frees the inhibitory sequence resulting in enhanced accessibility for C-subunit binding.

Removal of cAMP differentially affects the ϕ_{fast} values of the various sites examined. The ϕ_{fast} values of the more N-terminal sites examined (Thr^6Cys, Leu^{66}Cys, and Ser^{81}Cys) were unaffected by cAMP removal, however, the ϕ_{fast} values of the two sites in the cAMP-binding domains (FM-S145C and FM-S373C) were dramatically reduced. Additionally, the averaged emission lifetime of the FM-S99C mutant changed significantly upon removal of cAMP, indicating that cAMP affects the microenvironment of the reporter group at the Ser^{99}Cys site of mutation. These results indicate that low-nanosecond backbone fluctuations are tightly coupled within the cAMP-binding domains but not between the cAMP-binding domains and either the N-terminus or the interdomain.

It is important to note that the failure to detect ligand-induced changes in the ϕ_{fast} values does not mean that ligand binding has no effect on conformational flexibility. In the analysis of the effects of pseudosubstrate binding on the backbone flexibility around five sites of cysteine substitution in the C subunit, the ϕ_{fast} values of some sites did not change (*16*), although X-ray crystallographic results showed displacements of these same residues (*1*). This probably reflects the narrow time window (low nanosecond) of TRFA measurement and/or degree to which segmental moments are coupled within and between domains.

Although the degree of flexibility at the sites examined changes with C-subunit binding, the basic pattern of flexibility is retained (Figure 5). The ϕ_{fast} of FM-L66C was essentially unchanged with holoenzyme formation, indicating a retention of the apparent hinge segment on the C-terminal side of the D/D domain. The ϕ_{fast} of the structured interdomain mutant that could be examined (FM-S75C and FM-S81C) increased significantly, suggesting that this segment is more strongly associated with the C subunit than with the cAMP-binding domains. The one site in the cAMP-binding domains that could be examined (Ser^{373}Cys) appears to remain structured.

In summary, a combination of SDL and TRFA was used to both map the segmental flexibility of the R^I_α subunit and to examine the consequences of cAMP and C-subunit binding on its flexibility. The results suggest that there is a short hinge region, on the C-terminal side of the D/D domain, that is flexible in all configurations of the R^I_α subunit. The remainder of the interdomain region appears to be weakly associated with what is probably the tandem cAMP-binding domains. This interdomain segment becomes strongly associated with the C subunit upon holoenzyme formation. Also, there appears to be a "tight" coupling of the low-nanosecond fluctuations in the two disparate sites in the cAMP-binding domains examined, suggesting that all of the tandem cAMP-binding domain may be conformationally linked. Finally, cAMP binding selectively lowers the flexibility of the two sites examined in the tandem cAMP-binding domains and suggests that the structural stabilizing effects of cAMP are largely confined to these domains.

REFERENCES

1. Cox, S., Radzio-Andzelm, E., and Taylor, S. S. (1994) *Curr. Biol. 4*, 983−901.
2. Gangal, M., Cox, S., Lew, J., Clifford, T., Garrod, S. M., Aschbaher, M., Taylor, S. S., and Johnson, D. A. (1998) *Biochemistry 37*, 13728−13735.
3. Hauer, J. A., Taylor, S. S., and Johnson, D. A. (1999) *Biochemistry 38*, 6774−6780.
4. Léon, D. A., Dostmann, W. R. G., and Taylor, S. S. (1991) *Biochemistry 30*, 3035−3040.
5. Zhao, J., Hoye, E., Boylan, S., Walsh, D. A., and Trewhella, J. (1998) *J. Biol. Chem. 273*, 30448−30459.
6. Newlon, M. G., Roy, M., Morikis, D., Hausken, Z. E., Coghlan, V., Scott, J. D., and Jennings, P. A. (1999) *Nature (London) 6*, 222−227.
7. Su, Y., Dostmann, W. R. G., Herberg, F. W., Durick, K., Xuong, N.-h., Ten Eyck, L., Taylor, S. S., and Varughese, K. I. (1995) *Science 269*, 807−813.
8. Banky, P., Huang, L. J-.S., and Taylor, S. S. (1998) *J. Biol Chem. 3*, 5048−5055.
9. Herberg, F. W., Bell, S. M., and Taylor, S. S. (1993) *Protein Eng. 6*, 771−777.
10. Laemmli, U. K. (1970) *Nature 227*, 680−685.
11. Cook, P. F., Neville, M. E., Jr., Varana, K. E., Hartl, F. T., and Roskoski, R. Jr. (1982) *Biochemistry 21*, 5794−5799.
12. Hanson, D. C., Yguerabide, J., and Schumaker, V. N. (1981) *Biochemistry 20*, 6842−6852.
13. Beechem, J. M., Gratton, E., Ameloot, M., Knutson, J. R., and Brand, L. (1991) in *Topics in Fluorescence Spectroscopy* (Lakowicz, J. R., Ed.) Vol. 2, pp 241−305, Plenum Press, New York.
14. Buechler, Y. J., and Taylor, S. S. (1991) *J. Biol. Chem. 266*, 3491−3497.
15. Herberg, F. W., Taylor, S. S., and Dostmann, W. R. G. (1996) *Biochemistry 35*, 2934−2942.
16. Herberg, F. W., Dostmann, W. R. G., Zorn, M., Davis, S. J., and Taylor, S. S. (1994) *Biochemistry 33*, 7485−7494.
17. Gibson, R. M., Buechler, Y. J., and Taylor, S. S. (1997) *J. Biol Chem. 272*, 16343−16350.
18. Zheng, J., Knighton, D. R., Xuong, N. H., Ten Eyck, L. F., Karlsson, R., Xuong, N.-h., Taylor, S. S., and Sowadski, J. M. (1993) *Biochemistry 32*, 2154−2161.
19. Zheng, J., Knighton, D. R., Xuong, N. H., Taylor, S. S., Sowadski, J. M., and Ten Eyck, L. F. (1993) *Protein Sci. 2*, 1559−1573.
20. Gangal, M., Clifford, T., Deich, J., Cheng, X., Taylor, S. S., and Johnson, D. A. (1999) *Proc. Nat. Acad. Sci. U.S.A. 96*, 12394−12399.
21. Huang, L. J.-s., Durick, K., Weiner, J. A., Chun, J., and Taylor, S. S. (1997) *J. Biol. Chem. 272*, 8057−8064.

BI002196L